The Journal of Chemical Physics

Tuning the electronic band structure of metal surfaces for enhancing high-order harmonic generation

Cite as: J. Chem. Phys. **154**, 244702 (2021); https://doi.org/10.1063/5.0049532
Submitted: 05 March 2021 • Accepted: 10 June 2021 • Published Online: 23 June 2021

Hicham Agueny

The Journal of Chemical Physics ARTICLE scitation.org/journal/jcp

Tuning the electronic band structure of metal surfaces for enhancing high-order harmonic generation

Cite as: J. Chem. Phys. 154, 244702 (2021); doi: 10.1063/5.0049532
Submitted: 5 March 2021 • Accepted: 10 June 2021 •
Published Online: 23 June 2021

Hicham Agueny[a)]

AFFILIATIONS

Department of Physics and Technology, University of Bergen, Allegt. 55, N-5007 Bergen, Norway

[a)]Author to whom correspondence should be addressed: hicham.agueny@uib.no

ABSTRACT

High-harmonic generation (HHG) from the condensed matter phase holds promise to promote future cutting-edge research in the emerging field of attosecond nanoscopy. The key for the progress of the field relies on the capability of the existing schemes to enhance the harmonic yield and to push the photon energy cutoff to the extreme-ultraviolet (XUV, 10–100 eV) regime and beyond toward the spectral "water window" region (282–533 eV). Here, we demonstrate a coherent control scheme of HHG, which we show to give rise to quantum modulations in the XUV region. These modulations are shown to be caused by quantum-path interferences and are found to exhibit a strong sensitivity to the delocalized character of bulk states of the material. The control scheme is based on exploring surface states in transition-metal surfaces and, specifically, tuning the electronic structure of the metal surface itself together with the use of optimal chirped pulses. Moreover, we show that the use of such pulses having moderate intensities permits us to push the harmonic cutoff further to the spectral water window region and that the extension is found to be robust against the change in the intrinsic properties of the material. The scenario is numerically implemented using a minimal model by solving the time-dependent Schrödinger equation for the metal surface Cu(111) initially prepared in the surface state. Our findings elucidate the importance of metal surfaces for generating coherent isolated attosecond XUV and soft-x-ray pulses and for designing compact solid-state HHG devices.

I. INTRODUCTION

Coherent strong light–matter interaction has revolutionized our understanding of the properties of matter at the level of electrons.[1–6] It provides powerful tools for coherent control of quantum systems by exploiting light-induced non-linear processes. High-harmonic generation (HHG) is one such process. Due to its coherent aspect, it is routinely exploited in atomic and molecular gases to generate coherent extreme-ultraviolet (XUV) radiation and attosecond pulses[4,7,8] as well as to reveal the spectral and spatial characteristics of the electron motion.[9–11] The extension of the process to the condensed matter phase offers wider applicability. In particular, it promises to develop stable and highly efficient XUV and attosecond light sources in compact solid-state devices. This potential is motivated by the recent achievement of HHG from solid-state materials using laser pulses with a peak intensity of the order of 1 TW/cm^2. Such an intensity is too weak to generate high-order harmonics in the gas phase. In addition, solid-state HHG promises to promote future cutting-edge research in attosecond nanoscopy.[12–16] For instance, the possibility of accessing the electronic band structure of materials has been reported,[17,18] as well as their optical probing, as it allows us to access the crystal symmetry, interatomic bonding,[12,18,19] and phase diagram of the system.[20,21]

The HHG process in atomic and molecular gases is well established and understood on the basis of the semi-classical three-step model:[22,23] the ionized electrons via tunneling by means of a strong laser field, which after getting accelerated and, thus, acquiring extra energy, are driven back to recombine with the parent ion. Due to the presence of the oscillating field, the gained energy is converted into high-frequency radiation. This scenario occurs and repeats itself every half an optical cycle of the laser pulse, thus leading to the generation of coherent attosecond pulses. The coherent aspect of the generated pulses is determined by whether the consecutive harmonics are phase-locked and synchronized. In the HHG

spectrum, the process manifests by the appearance of harmonic components located at the multiples of the fundamental laser frequency depending on the symmetry of the involved interactions and is characterized by the harmonic cutoff.

In solid-state systems, the process is, however, more complicated, and the intuitive atomic-based models are often incomplete and do not hold for properly describing the solid-state HHG. The complexity is due to the involved interband and intraband mechanisms,[13,24–27] in which their role for generating high-order harmonics is still under debate.[13,28] The origin of these two types of mechanisms is understood to be caused by distinct dynamical effects:[13,18,29,30] the interband dynamics[13] is found to be associated with the recollision of an electron–hole pair generated by means of an oscillating field, which results in the emission of high-harmonic photons, whereas the intraband mechanism[30] is linked to the dynamical Bloch oscillations, in which electron or hole carriers oscillate in the Brillouin zone under the action of laser fields. Here, some studies have primarily considered either of the above-mentioned mechanisms (e.g., Refs. 12, 28, and 31). In particular, it has been discussed that at long wavelength laser pulses (i.e., in the range 1–5 μm), the contribution of the interband mechanism dominates the HHG process.[32]

In general, pushing the high-energy cutoff region to higher photon energies covering the XUV (10–100 eV) and water window (282–533 eV) spectral regimes and enhancing the corresponding yields are one of the challenges of the HHG process.[8,33,34] Generating coherent radiation in these spectral regimes, which consists of isolated attosecond pulses (IAPs),[35,36] is motivated by their potential use for time-resolved applications in chemical and materials sciences.[8,33,37] In particular, these IAPs have the potential to localize the coherent motion of a wavepacket at a specific site in molecules and solid-state systems, thus offering the opportunity for resolving structural changes occurring during photo-chemical and biological processes as well as phase transition in insulator-to-metal materials with an unprecedented temporal resolution.

The last decade has marked the first experimental observations of solid-state HHG,[12,13,17–19,24] which, in turn, have sparked off extensive theoretical works (e.g., Refs. 27 and 38–43) to further understand the origin of the process and to investigate the possibility of enhancing its efficiency. These theoretical considerations were mostly focused on HHG from bulk semiconductors, in which the electron wavepacket is initially delocalized over bulk states. In these works, the generated harmonics were limited to lower-order regions and up to the order 25th, and the used laser intensities, although operate in the non-perturbative regime, cannot be too high to prevent the material from damage. Alternative studies address the HHG from metal surfaces Cu(111) and precisely from the surface state, in which the electron wavepacket is initially localized and the control scheme explores the effect of growing ultrathin layers of the insulator NaCl on single-crystal metal surfaces.[44] In this context, recent works have focused on implementing different strategies for enhancing the HHG process. Example schemes include tuning the electronic structure and carrier injection as in the experiment[45] or by theoretically investigating the effect of doping[42,46] or vacancy defects.[47,48]

In this work, we pursue the aim of establishing coherent control schemes with the capability of improving the efficiency of solid-state HHG and toward the generation of coherent XUV and soft-x-ray pulses. At this end, we systematically explore the sensitivity of the HHG process from the transition-metal surface Cu(111) and specifically from surface states to the spectral properties of chirped laser pulses and to those of the electronic structure of the metal surface itself. The particularity of surface states relies on the characteristic of being located at the outermost atomic surface layers, rendering them easier to be manipulated.[49] This, in turn, affects the physical and chemical properties at the interfaces, and this makes the interaction with transition metals (see, e.g., Refs. 50–53) of particular importance for studying chemical processes.[50,54,55]

We, thus, explore HHG from surface states for examining the possibility of extending the harmonic cutoff to the XUV and soft-x-ray regions and simultaneously enhancing the corresponding harmonic yields. This is shown to be achieved on the basis of numerical simulations of the time-dependent Schrödinger equations (TDSEs) using a minimal model. In particular, we show that tuning the chirp parameters of the pulse allows one to significantly extend the harmonic cutoff to access the spectral water window region, i.e., from the 15th harmonic in the free-chirp case to the 550th harmonic in the case of an optimized chirped pulse having moderate intensities. Further analysis reveals an enhancement of the harmonic yield accompanied by spectral modulations in the XUV photon energy region (i.e., in the range of 69th and 79th harmonics), unlike previous studies, in which the modulations were observed at lower-order harmonics (i.e., seventh and nineth harmonics)[56] generated from bulk crystals using a free-chirp pulse. We further show that the observed modulations originate from quantum-path interference[57,58] of electrons characterized by short and long travel times, which leads to the generation of photons having the same final energy. We validate these observations using a simple physical model that captures the quantum aspect of the modulations. These modulations, in turn, are found to exhibit a strong sensitivity to the change in the number of Cu monolayers (MLs), while beyond the XUV region, the HHG spectra remain unchanged. We exploit this sensitivity for coherent control of the HHG process by selectively manipulating the bulk states combined with the use of optimal chirped pulses. Our findings, thus, indicate the importance of exploring metal surfaces for the generation and characterization of IAPs in the XUV and soft-x-ray regimes, thus bridging the gap between attosecond and surface sciences.

This paper is organized as follows: In Sec. II, we present our theoretical model based on a one-dimensional (1D)-TDSE, including a short description of our numerical methods for solving the TDSE and for calculating the HHG spectrum. We stress that extensive theoretical works have been carried out using a 1D model, which was shown to capture the basic physics involved in an experiment (e.g., Ref. 59). In Sec. III, we present our results of HHG spectra produced by chirped pulses and explore the role of bulk states to coherently control the HHG process from the surface state of Cu(111) and discuss the physics behind the emerged effects. We also predict the generation of IAPs in the XUV and soft-x-ray photon energy regions, which can be characterized via the chirp parameter of the pulse and the metal surface itself. The findings are supported by an analysis of the calculated population of the bulk, image, and surface states as well as the use of a simple physical model. Finally, in Sec. IV, we summarize our results of HHG. Atomic units (a.u.) are used throughout this paper unless otherwise specified.

II. THEORY AND COMPUTATIONAL DETAILS

The electron dynamics induced inside metal surfaces is modeled using a 1D model with the use of a one-electron pseudopotential as in previous works.[44,59,60] In a 3D model, the metal surface electron feels the potential in the direction normal to the surface, while it is considered to move freely with the electron momentum $k_{\parallel}$ in the parallel direction. This justifies our restriction to the one-direction motion of the electron, which is here triggered by a linearly polarized laser pulse directed to the (111) direction of the metal surface. On the basis of this 1D model, the TDSE governing the electron dynamics induced by coherent light pulses is written as

$$\left[-\frac{\nabla_z^2}{2} + V_{ion}(z) + H_I(t) - i\frac{\partial}{\partial t}\right]|\psi(t)\rangle = 0, \tag{1}$$

where $V_{ion}(z)$ is an effective potential interaction. Here, we use Chulkov potentials to model the electronic structures of the metal surface Cu(111). The potentials are parameterized and have the analytical form[61]

$$V_1(z) = A_{10} + A_1\cos\left(\frac{2\pi}{a_s}z\right), \quad z < 0, \tag{2a}$$

$$V_2(z) = -A_{20} + A_2\cos(\gamma z), \quad 0 < z < z_1, \tag{2b}$$

$$V_3(z) = A_3\exp[-\alpha(z - z_1)], \quad z_1 < z < z_{im}, \tag{2c}$$

$$V_4(z) = \frac{\exp[-\lambda(z - z_{im})] - 1}{4(z - z_{im})}, \quad z_{im} < z, \tag{2d}$$

where a_s is the bulk interlayer spacing and z_{im} is the position of the image plane. The parameters A_{10}, A_1, A_2, and β are independent parameters and are given in Table I for the metal surface Cu(111). They are adjustable and are obtained using a fitting procedure involving results from the density function calculations and experiments.[61] While the parameters A_{20}, A_3, α, z_1, λ, and z_{im} are determined from the continuity condition of the potential and its first derivative and are given according to[61,62]

$$\begin{aligned} A_{20} &= A_2 - A_{10} - A_1, \quad A_3 = -A_{20} - \frac{A_2}{\sqrt{2}}, \\ z_i &= \frac{5\pi}{4\gamma}, \quad \alpha = \frac{A_2\gamma}{A_3}\sin(z_1\gamma), \\ \lambda &= 2\alpha, \quad z_{im} = z_1 - \frac{1}{\alpha}\ln\left(-\frac{\alpha}{2A_3}\right). \end{aligned} \tag{3}$$

Note that the pseudopotential in Eq. (2) is multiplied by a damping function of the form $[1 + \tanh(z)]/2$, similar to that used in Ref. 44, to ensure the continuity of the potential at the boundaries. The time-dependent interaction $H_I(t)$ in Eq. (1) is treated in the length gauge and is described within the dipole approximation according to

$$H_I(t) = -zS(z)F(t) = S(z)E_0 f(t)\cos(\omega_0 t + \phi(t)), \tag{4}$$

where the function $S(z)$ accounts for screening of the electric field inside the Cu(111) surface (see, e.g., Refs. 44 and 59) and takes the form

$$S(z) = 0.5\{1 + \tanh[6z + 3\xi)/\xi]\}. \tag{5}$$

Here, ξ is the screening length. We have performed calculations for $\xi = 4$, 10, and 20. Our results are not very sensitive to the change in ξ. The function $f(t)$ in Eq. (4) is the pulse envelope that is chosen to be of a cosine square form, ω_0 is the central angular frequency, and E_0 is the peak amplitude of the laser pulse and is related to the peak intensity via the relation $I_0 = E_0^2$. The function $\phi(t)$ in Eq. (4), which is a time-dependent carrier-envelope phase (CEP), determines the form of the chirped pulse. In this work, we use a chirped pulse similar to the one in Ref. 63, whose phase $\phi(t)$ has the following time-varying profile:

$$\phi(t) = -\beta\tanh\left(\frac{t - t_0}{\tau}\right), \tag{6}$$

and the corresponding instantaneous frequency is obtained according to

$$\omega(t) = \omega_0 - \frac{d\phi(t)}{dt} = \omega_0 - \frac{\beta}{\tau}\left[\cosh^2\left(\frac{t - t_0}{\tau}\right)\right]^{-1}, \tag{7}$$

where the chirp parameters β (given in rad) and τ can be adjusted to control, respectively, the frequency sweeping range and the steepness of the chirped pulse centered at t_0. In Eqs. (6) and (7), the optical phase $\phi(t)$ becomes zero in the case of $\beta = 0$, and thus, we have $\omega(t) = \omega_0$; this defines the chirp-free case.

As we use a hyperbolic chirp, the chirp parameter β can be interpreted as a hyperbolic chirp rate. Thus, the values of β we consider in our work mean different rates at which the instantaneous frequency changes, which, in turn, should result in a dramatic change in HHG spectra as we will show. A detailed description of the chirp rate β and how it relates to the dispersion coefficients is provided in the supplementary material.

As in our previous work,[64] we calculate the HHG spectrum $H(\omega)$ by carrying out the Fourier transform of the expectation value of the dipole acceleration along the z-axis,

$$H(\omega) = |D_z(\omega)|^2, \tag{8}$$

where $D_z(\omega)$ is defined by

$$D_z(\omega) = \frac{1}{\sqrt{2\pi}}\int_{t_i}^{t_f}\langle D_z(t)\rangle e^{-i\omega t}dt, \tag{9}$$

and the time-dependent expectation value of the dipole acceleration $\langle D_z(t)\rangle$ is written as

TABLE I. Adjustable parameters used in the analytical pseudopotential in Eq. (2), which is shown in Fig. 1(a). The values are taken from Ref. 61. All parameters are given in atomic units.

a_s	A_{10}	A_1	A_2	γ
3.94	−0.4371	0.1889	0.1590	2.9416

$$D_z(t) = \langle\psi(t)|\frac{\partial V(r)}{\partial z} + F(t)|\psi(t)\rangle. \quad (10)$$

In Eq. (9), t_i and t_f define, respectively, the time at which the pulse is switched on and off. Note that the dipole acceleration $\langle D_z(t)\rangle$ in Eq. (10) is convoluted by a window function of a Gaussian form $\exp[-(t-t_0)^2/(2\sigma^2)]$ centered at t_0 and having a width of $\sigma = 5.77/\omega_0$.

In our numerical simulations, the initial states are obtained by diagonalizing the matrix representation of the Hamiltonian in Eq. (1) in the absence of the laser pulse, which is constructed using of a sinus-DVR (discrete variable representation) basis.[65] The time evolution of the electronic wave function $\psi(t)$, which satisfies the TDSE [cf. Eq. (1)], is solved numerically using a split-operator method combined with a fast Fourier transform (FFT) algorithm. The calculations are carried out in a grid of size $L_z = 8190$ with the spacing grid $dz = 0.25$ a.u., i.e., $n_z = 32\,768$ grid points. The time step used in the simulation is $\delta t = 0.02$ a.u. The convergence is checked by performing additional calculations with twice the size of the box and a smaller time step. An absorbing boundary is employed to avoid artificial reflections, but without perturbing the inner part of the wave function. The boundary is chosen to span 10% of the grid size in the z-direction.

III. RESULTS AND DISCUSSION

The control scheme implemented in this work is based on tuning the electronic structure of the metal surface itself combined with the search of optimal parameters of the chirped pulse. The main goal is to investigate the possibility of extending the harmonic cutoff with simultaneous enhancement of the harmonic yield. This is achieved using a simple physical model, in which we incorporate a pseudopotential that has been widely used to study, for instance, HHG[44] and time-resolved photoemission.[66] It was found that the model captures the basic physics involved in an experiment (e.g., Refs. 59 and 67). Here, we use the metal surface Cu(111), which is considered to be initially prepared in the surface state having an energy of −5.33 eV. The energy is located in the forbidden energy gap and below the Fermi level ($E_f = -4.5$ eV), as depicted in Fig. 1(b). The electron density of the corresponding state is shown in Fig. 1(a) (green curve) and exhibits a localized character close to the surface atomic layer and decays into both the vacuum and the bulk,[49] unlike bulk states that have a Bloch character and the corresponding electron density is delocalized over the bulk metal and decays into the vacuum, as depicted in Fig. 1(a) (orange curve). We, thus, exploit this characteristic feature of the surface state for coherent control of the HHG process.

In Fig. 2, we show HHG spectra generated by chirped near-infrared pulses. The pulse is characterized by a chirp parameter β and has a 1.27 μm central wavelength, 43 fs pulse duration, and 2×10^{13} W/cm^2 as the maximum of the peak intensity. The choice of the pulse intensity is limited by the material damage, as discussed in Ref. 44. Figure 2(a) shows a strong sensitivity of the spectrum to the change in the chirp parameter β. Here, the parameter β covers the region 0–10.8 rad. The choice of these values is such that the instantaneous frequency $\omega(t)$ remains positive. Note that only the positive chirps affect the HHG spectrum. The range of β considered in our work covers a large number of optimal parameters that enable us to achieve a high degree of control and efficiency of the HHG. Varying the chirp parameter β means varying the instantaneous frequency of the chirped light pulses [cf. Eq. (7)]. For an optimal parameter of β, the instantaneous frequency $\omega(t)$ becomes very small close to the center of the pulse, which results in a high pondermotive energy $U_p = I/4\omega^2(\beta)$ acquired by the free electron in an oscillating field [cf. Eq. (11)]. The U_p determines the extension of the harmonic cutoff. Therefore, we search for parameters β that are optimal for selectively enhancing the harmonic yield and simultaneously extending the harmonic cutoff to cover the XUV and soft-x-ray photon energy regions. Generating isolated attosecond pulses in these regions is desirable in attosecond science.

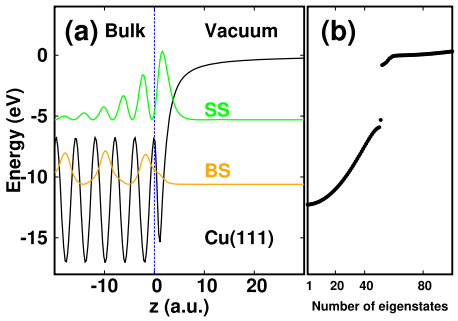

FIG. 1. (a) Effective one-dimensional potential (black curve) and the electron densities of the surface state labeled SS having an energy of −5.3 eV and a bulk state (BS) with an energy of −10.6 eV for Cu(111). The electron densities of the SS and BS are multiplied by 30 and 200, respectively. (b) Eigenenergy at $k_\parallel = 0$ of the binding electronic states of the model potential in (a). Here, $k_\parallel$ is the crystal momentum of the electron. The pseudopotential is plotted in the limited range [−20:30] (a.u.) along the z-axis, and the derivative of the potential is continuous (see the text).

In the range of β considered in Fig. 2, the energy cutoff extends from $E_{max} = 15$ eV for $\beta = 0$ (free-chirp case) to $E_{max} = 540$ eV for $\beta = 10.4$. An extension by almost a factor of 36 is observed. The increase in the energy cutoff E_{max} as a function of increasing the chirp β is found to follow the approximative formula

$$E_{max}(\beta) = I_p + 3.17U_p(\beta), \quad (11)$$

as depicted in Fig. 2(a) with the white curve. Here, I_p is the ionization potential. The instantaneous frequency $\omega(t)$, which is a time-dependent function [cf. Eq. (7)], is found to be determined at times defined as $t = e^{1.45\sqrt{\beta}}$. By introducing this latter formula, Eq. (11), although deviates from the well known one in the free-chirp case [see the horizontal white line in Fig. 2(a)], is found to reproduce very well the energy cutoff in the whole range of the chirp parameter. On the other hand, Eq. (11) captures the basic physics behind the significant extension of the cutoff region. It shows that the free electrons acquire high-kinetic energy from the field, which is inversely proportional to the instantaneous frequency characterized by the chirp parameter. Indeed, increasing the parameter β results in decreasing the instantaneous frequency $\omega(t)$, and hence, a vast kinetic energy $U_p(\beta)$ up to 170 eV is transferred to the free electrons compared to 3 eV in the free-chirp case.

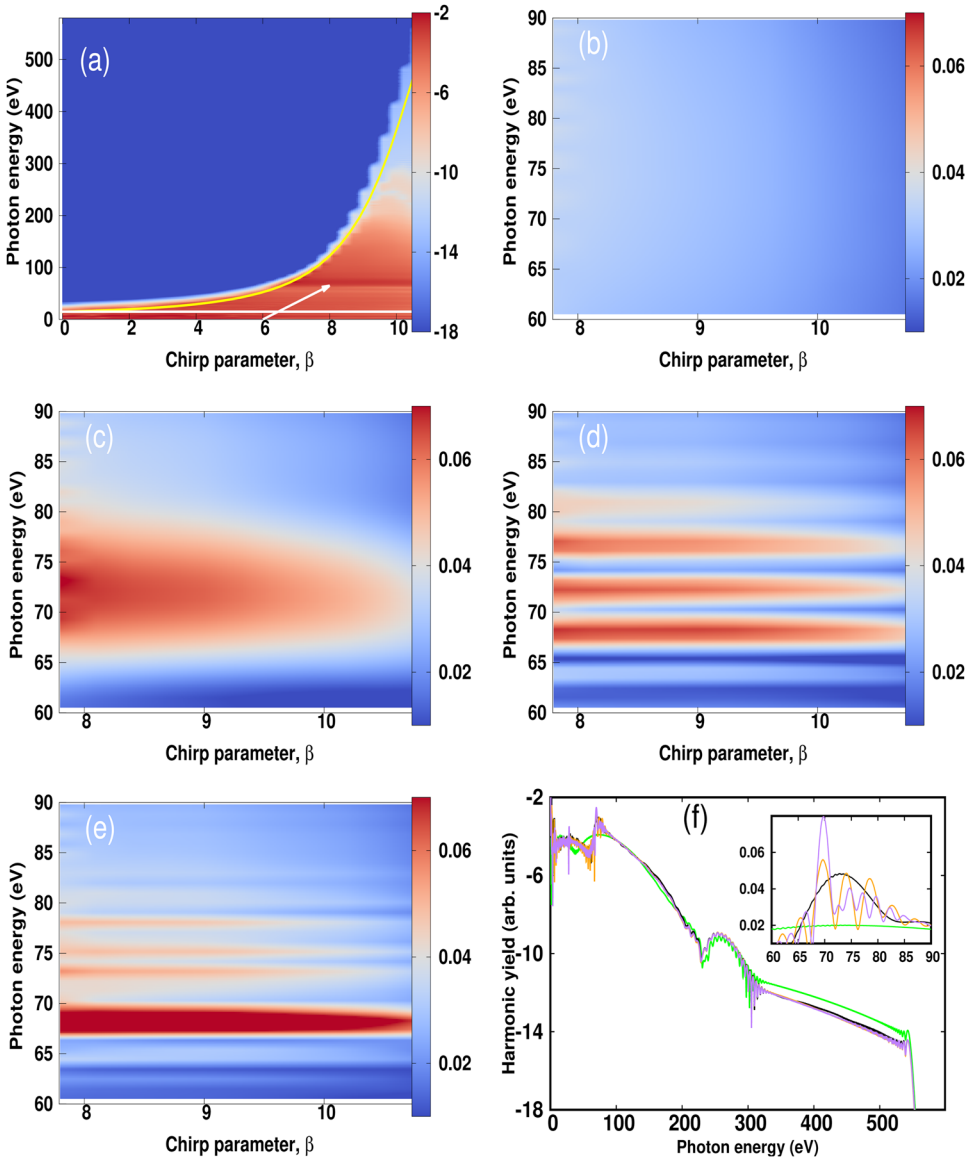

FIG. 2. (a) HHG spectra calculated from the Cu(111) surface state with 10 MLs as a function of the chirp parameter β in the range 0–10.8 rad. The yellow curve in (a) displays the cutoff energy deduced from Eq. (11), and the horizontal white line corresponds to the free-chirp case. [(b)–(e)] The same as (a), but the spectra are displayed in the XUV region as indicated by the arrow in (a) and for β in the range 7.7–10.8 rad and at a various number of MLs: (b) 1 ML, (c) 10 MLs, (d), 30 MLs, and (e) 50 MLs. (f) HHG spectra for β = 10.4 rad at different MLs: 1 ML (green curve), 10 MLs (orange curve), 30 MLs (purple curve), and 50 MLs (black curve). Inset: a zoomed-in image of the spectra in (f) in the XUV region. The parameters of the chirped pulse are λ_{NIR} = 1.27 μm, T_c = 10 cycles, τ = 300 a.u., and I_{NIR} = 2 $\times 10^{13}$ W/cm^2.

A closer inspection of the HHG spectrum shows an enhancement of the harmonic yield in the photon energy region 60–90 eV at the optimal chirp parameter range 7–10.8 rad, as indicated by the arrow in Fig. 2(a). The spectra in these ranges are displayed with higher visibility in Figs. 2(b)–2(e) at various Cu MLs, respectively, 1, 10, 30, and 50 MLs. Interestingly, varying the number of MLs of the metal surface itself results in an abrupt change in the spectrum. The change here manifests by spectral modulations, in particular, at 30 and 50 MLs, while these modulations are absent in the case of 10 MLs, in which only an enhancement of the harmonic yield is seen. On the other hand, no changes in the spectrum are observed in the case of 1 ML. This sensitivity of HHG to the change in MLs is mainly seen in the photon energy region 60–90 eV, while beyond this region, the curves of the spectrum fall on the top of each other except in the case of 1 ML, in which a slight difference is noted. On the other hand, the harmonic cutoff remains unchanged, as can be seen in Fig. 2(f). In Fig. 2(f), the spectra are shown for the chip parameter β = 10.4 rad, and a zoomed-in image of the spectrum in

the XUV photon energy region is displayed as an inset to highlight the emerged modulations.

These results indicate that by properly choosing the chirp parameter, one can produce high-energy photons covering the spectral water range 283–533 eV. On the other hand, tuning the electronic band structure by varying the number of MLs results in an enhancement of the harmonic yield in the XUV photon energy region accompanied by spectral modulations. Such an enhancement is only possible when introducing an optimal chirped pulse, which here plays a role in switching on/off the access to bulk states. As a result, manipulating these states by tuning the MLs of the metal surface itself leads to a dramatic change in the HHG process. Here, increasing the number of MLs leads to the generation of a large number of bulk states, which get involved in the dynamics induced by the chirped pulse. This can be seen in Fig. 3, in which we show the population of the bulk states (red curve), surface state (black curve), and image states (orange curve) as well as the probability of the total excitation (green curve) and the ionization (purple curve) as functions of the chirp parameter β. These results are presented at different MLs: 1, 10, 30, and 50 MLs. At the first glance, the excitation exhibits a strong sensitivity to the change in the number of MLs. Note that in the case of 50 MLs, there are 50 bulk states located below the surface state and only 10 bulk states in the case of 10 MLs, while no bulk state exists when only 1 ML is considered. Here, the total excitation results from the contribution of bulk states, which is significant except in the case of 1 ML, in which the excitation comes from the contribution of image states. On the contrary, the ionization probability is slightly affected by the change in the number of MLs, which indicate that the implemented control scheme modifies mainly the phase dipole emission.

To provide further insights into the origin of these modulations, we show in Fig. 4(a) the phase information ϕ of each harmonic extracted from Eq. (9). This phase is shown for $\beta = 10.4$ rad and is displayed at a various number of MLs: 1 ML (orange curve), 10 MLs (purple curve), 30 MLs (green curve), and 50 MLs (black curve). Note that the magnitude of the phases is shown with an offset to allow a direct comparison between different results. In Fig. 4(a), an abrupt change in the phase dipole is seen at 30 and 50 MLs, while this behavior is absent in the case of 1 and 10 MLs. This is consistent with the observed spectral modulations in Figs. 2(d) and 2(e) and their absence in Figs. 2(b) and 2(c). These observations demonstrate the quantum nature of the modulations, which are further validated by a simple physical model derived from the semi-classical approximation[68] given by

$$H_q(\omega_q) = \int dt e^{-i\omega_q t}\left[\int_{-\infty}^{t} dt' d_z(t')F(t')e^{i\phi_q(t,t')}\right]. \quad (12)$$

Here, the phase $\phi_q(t,t') = -S(t,t') + \Delta E t'$ contains the classic action $S(t)$ and the energy difference ΔE involving a specific

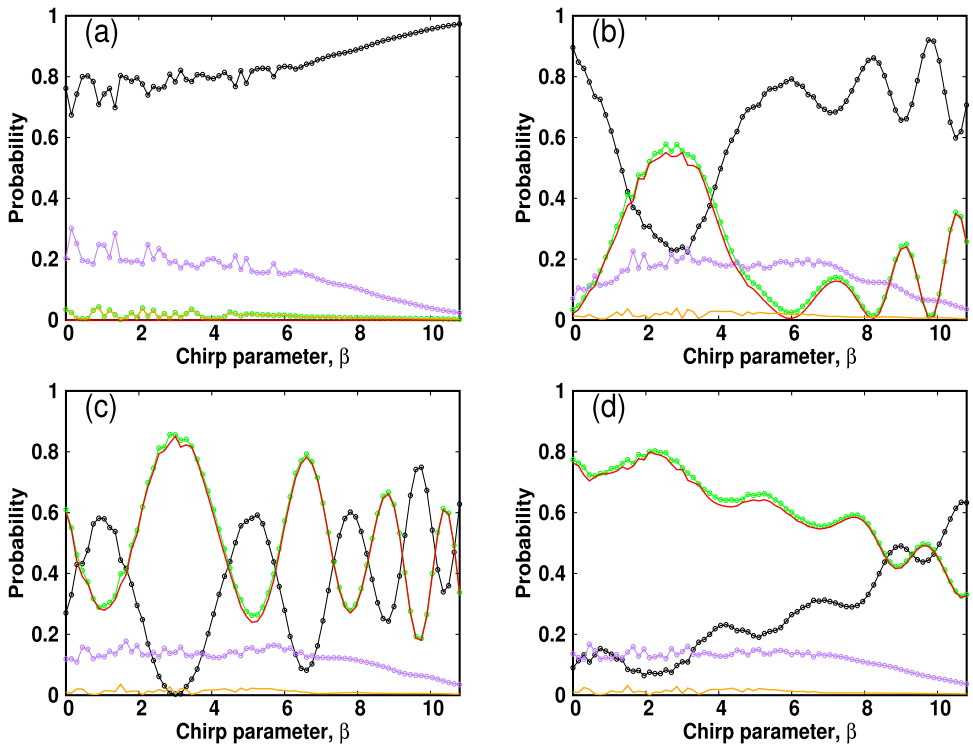

FIG. 3. Probability of occupied states as a function of the chirp parameter β at a various number of MLs: (a) 1 ML, (b) 10 MLs, (c) 30 MLs, and (d) 50 MLs. The population is shown for the initial state (black curve with circles), bulk states (red curve), and image states (orange curve). Also shown are the probability of the excitation (green curve with circles) and the ionization (purple curve with circles). The parameters of the chirped pulse are $\lambda_{NIR} = 1.27\ \mu$m, $T_c = 10$ cycles, $\tau = 300$ a.u., and $I_{NIR} = 2 \times 10^{13}$ W/cm^2.

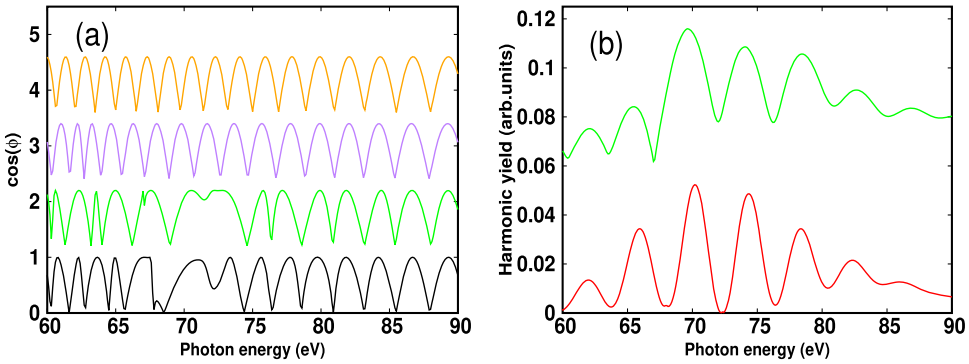

FIG. 4. (a) Phase ϕ of the harmonics in the XUV region at a various number of MLs: 1 ML (orange curve), 10 MLs (green curve), 30 MLs (purple curve), and 50 MLs (black curve). (b) Harmonics calculated from a simple physical model in Eq. (14) (see the text) (red curve). For reference, the HHG spectrum obtained with 30 MLs is also shown with a green curve and with an offset. The parameters of the chirped pulse are λ_{NIR} = 1.27 μm, T_c = 10 cycles, β = 10.4 rad, τ = 300 a.u., and I_{NIR} = 2 $\times 10^{13}$ W/cm^2.

transition, $d_z(t')$ is the transition dipole moment, and $F(t')$ is the electric field. The expression in Eq. (12) illustrates that each harmonic q results from a coherent sum of dipole emission amplitudes augmented by the phase ϕ_q. In a semi-classical picture, this coherent sum involves short and long trajectories followed by the electron during the recombination process.[68,69] It should be noted that our goal here is not to evaluate the integral in Eq. (12) exactly but rather to provide a simple physical model that captures the basic physics involved in the exact TDSE calculations. At this end, we simplify the expression above by assuming that at each time t of the pulse, the integral over t' is dominated by two trajectories represented by the amplitude $a_i(t)$ and the phase $\phi_i(t)$ $(i = s, l)$, where the labels s and l refer, respectively, to the short and long trajectories. Using this assumption leads to

$$H_q(\omega_q) = \int \mathrm{d}t e^{-i\omega_q t}\left[a_s(t)e^{i\phi_s(t)} + a_l(t)e^{i\phi_l(t)}\right], \tag{13}$$

which can be further simplified as

$$H_q(\omega_q) = a_s(\omega_q)e^{-i(\Delta\phi_q - \omega_q t_s)} + a_l(\omega_q)e^{i\omega_q t_l}. \tag{14}$$

Here, $\Delta\phi_q$ is the relative phase between the amplitudes a_s and a_l. The times t_s and t_l refer to the short and long travel times of the electron in the continuum. To evaluate the quantity in Eq. (14), we assume that the amplitudes a_i have a Gaussian form $\exp[-\frac{(\omega_q-\omega_i)^2}{2\sigma_i^2}]$ centered around the photon energy of ω_i and characterized by the width σ_i. The parameters $\Delta\phi_q$, σ_i, and t_i are obtained by fitting the model in Eq. (14) to the TDSE data. The result stemming from this model is shown in Fig. 4(b) with a red curve and is found to reproduce very well the oscillations imprinted in the spectrum obtained from the exact TDSE calculations. The close agreement between the analytical model in Eq. (14) and the TDSE calculations demonstrates the origin of the spectral modulations as a result of quantum interference between short and long trajectories followed by the electron during the recombination, which leads to the generation of photons with the same final energy. The emerged quantum interference effects manifest by spectral modulations in HHG spectra and are of particular interest since they appear in the XUV energy range. This is an interesting finding, which can be exploited for generating isolated attosecond XUV pulses with enhanced intensities. On the other hand, the sensitivity of the generated photons to the number of bulk states is a signature of a coherent control of the HHG process. This sensitivity can be understood in the following: during the recombination process, the electron wavepacket, which is initially localized close to the surface, recollides not only with surface states but also with different bulk states. These bulk states possess a delocalized character, which makes them a source of additional recollision events, thus contributing to the efficiency of the HHG process. Therefore, the observed pattern in HHG spectra encodes information about the electronic structure of the metal surface, and this makes high-order harmonic spectroscopy induced by means of chirped pulses a powerful characterization tool of materials. Our work, therefore, introduces a new scheme for coherent control of solid-state HHG that combines the use of optimal chirped pulses with the ability to tune the electronic band of the material itself. This, indeed, is the key ingredient for inducing quantum-path interferences, thus achieving a high degree of control and efficiency of HHG.

Producing chirped femtosecond pulses should be possible using the current state-of-the-art techniques, which benefit from the nowadays ultrafast laser technologies (e.g., Ref. 70). A widely used technique that is considered as a standard laser configuration is the chirped pulse amplification,[71] which is based on the stretching and compression of the laser pulse. In this technique, the control of the chirped pulse can be achieved using, for instance, active devices such as deformable mirrors or liquid crystal arrays.[72,73] On the other hand, generating a positive chirp, as in our work, can be done in an experiment using an imperfect dispersion compensation,[73] which can be achieved by tuning either a pulse stretcher or a pulse compressor. Furthermore, the characterization of the chirped pulse can be realized using frequency-resolved optical gating technique.[74] We, thus, believe that the coherent control scheme proposed in our work, which exploits quantum-path interference to enhance both the yield and the harmonic cutoff of HHG, should be experimentally feasible.

IV. CONCLUSIONS

In conclusion, we have demonstrated the efficiency of a coherent control scheme applied to enhance HHG from the transition-metal surface Cu(111). This was shown to be achieved on the basis of numerical simulations of the time-dependent Schrödinger equation using a minimal model. Besides showing the extension of the harmonic cutoff by almost a factor of 36, we have demonstrated a control scheme in which the chirped pulse acts as an on/off switch for accessing bulk states, which when getting selectively manipulated by tuning the intrinsic properties of the metal surface itself gives rise to quantum modulations in the XUV photon energy region. These emerged quantum effects were linked to the interference between short and long trajectories followed by electrons during the recombination process, which leads to the generation of photons with the same final energy. This interpretation was validated using a simple physical model that contains the basic ingredients necessary for understanding the origin of the quantum nature of the observed effects, thus providing new insights into the solid-state HHG. Furthermore, it was found that these quantum modulations exhibit a strong sensitivity to the delocalized character of bulk states, although the electron dynamics was initiated from the localized surface state. This illustrates the fundamental role of the delocalization aspect of states that characterizes solid-state systems, which can be exploited for coherent control of the HHG process. On the other hand, these results indicate that the process encodes information about the intrinsic properties of the material under consideration.

We stress here that the role of the localization of the electron wavepacket in solid-state HHG has been discussed recently with the use of a Wannier–Bloch approach.[31] The approach is based on the conventional atomic picture, in which the electron wavepacket is considered to be localized in an individual atomic site of the periodic lattice of a ZnO crystal, and its contribution to HHG was evaluated. In our model, however, the dynamics is initiated from the surface state of the metal surface Cu, in which the electron is initially localized. Therefore, it is clear that both scenarios are different in terms of the considered material, the nature of the used light pulses and the physics behind the emerged effects in HHG spectra. Our findings, thus, provide new insights into the role of the delocalization nature of bulk states for inducing quantum-path interferences when it combines with the use of chirped pulses. On the other hand, our results suggest the use of chirped pulses for spectral characterization of bulk states via high-order harmonic spectroscopy. Most importantly, the results indicate the relevance of metal surfaces when combined with the use of chirped pulses for advancing attosecond science and potentially for developing compact solid-state based HHG devices.

SUPPLEMENTARY MATERIAL

See the supplementary material for a detailed description of the chirp rate and how it relates to the dispersion coefficients.

ACKNOWLEDGMENTS

The author would like to thank Dr. Abdelmalek Taoutioui for fruitful discussions.

DATA AVAILABILITY

The data that support the findings of this study are available from the corresponding author upon reasonable request.

REFERENCES

[1] A. H. Zewail, "Laser femtochemistry," Science **242**, 1645–1653 (1988).
[2] A. Mokhtari, P. Cong, J. L. Herek, and A. H. Zewail, "Direct femtosecond mapping of trajectories in a chemical reaction," Nature **348**, 225–227 (1990).
[3] M. Shapiro and P. Brumer, "Coherent control of atomic, molecular, and electronic processes," in *Advances in Atomic, Molecular, and Optical Physics* (Academic Press, 2000), pp. 287–345.
[4] P. B. Corkum and F. Krausz, "Attosecond science," Nat. Phys. **3**, 381–387 (2007).
[5] A. H. Zewail, "Four-dimensional electron microscopy," Science **328**, 187–193 (2010).
[6] A. Frisk Kockum, A. Miranowicz, S. De Liberato, S. Savasta, and F. Nori, "Ultrastrong coupling between light and matter," Nat. Rev. Phys. **1**, 19–40 (2019).
[7] F. Krausz and M. Ivanov, "Attosecond physics," Rev. Mod. Phys. **81**, 163–234 (2009).
[8] J. Li, J. Lu, A. Chew, S. Han, J. Li, Y. Wu, H. Wang, S. Ghimire, and Z. Chang, "Attosecond science based on high harmonic generation from gases and solids," Nat. Commun. **11**, 2748 (2020).
[9] J. Itatani, J. Levesque, D. Zeidler, H. Niikura, H. Pépin, J. C. Kieffer, P. B. Corkum, and D. M. Villeneuve, "Tomographic imaging of molecular orbitals," Nature **432**, 867–871 (2004).
[10] B. K. McFarland, J. P. Farrell, P. H. Bucksbaum, and M. Gühr, "High harmonic generation from multiple orbitals in N_2," Science **322**, 1232–1235 (2008).
[11] A. J. Uzan, H. Soifer, O. Pedatzur, A. Clergerie, S. Larroque, B. D. Bruner, B. Pons, M. Ivanov, O. Smirnova, and N. Dudovich, "Spatial molecular interferometry via multidimensional high-harmonic spectroscopy," Nat. Photonics **14**, 188–194 (2020).
[12] S. Ghimire, A. D. DiChiara, E. Sistrunk, P. Agostini, L. F. DiMauro, and D. A. Reis, "Observation of high-order harmonic generation in a bulk crystal," Nat. Phys. **7**, 138–141 (2011).
[13] G. Vampa, T. J. Hammond, N. Thiré, B. E. Schmidt, F. Légaré, C. R. McDonald, T. Brabec, and P. B. Corkum, "Linking high harmonics from gases and solids," Nature **522**, 462–464 (2015).
[14] M. F. Ciappina, J. A. Pérez-Hernández, A. S. Landsman, W. A. Okell, S. Zherebtsov, B. Förg, J. Schötz, L. Seiffert, T. Fennel, T. Shaaran, T. Zimmermann, A. Chacón, R. Guichard, A. Zaïr, J. W. G. Tisch, J. P. Marangos, T. Witting, A. Braun, S. A. Maier, L. Roso, M. Krüger, P. Hommelhoff, M. F. Kling, F. Krausz, and M. Lewenstein, "Attosecond physics at the nanoscale," Rep. Prog. Phys. **80**, 054401 (2017).
[15] G. Vampa and T. Brabec, "Merge of high harmonic generation from gases and solids and its implications for attosecond science," J. Phys. B: At., Mol. Opt. Phys. **50**, 083001 (2017).
[16] H. Lakhotia, H. Y. Kim, M. Zhan, S. Hu, S. Meng, and E. Goulielmakis, "Laser picoscopy of valence electrons in solids," Nature **583**, 55–59 (2020).
[17] M. Hohenleutner, F. Langer, O. Schubert, M. Knorr, U. Huttner, S. W. Koch, M. Kira, and R. Huber, "Real-time observation of interfering crystal electrons in high-harmonic generation," Nature **523**, 572–575 (2015).
[18] G. Vampa, T. J. Hammond, N. Thiré, B. E. Schmidt, F. Légaré, C. R. McDonald, T. Brabec, D. D. Klug, and P. B. Corkum, "All-optical reconstruction of crystal band structure," Phys. Rev. Lett. **115**, 193603 (2015).
[19] Y. S. You, D. A. Reis, and S. Ghimire, "Anisotropic high-harmonic generation in bulk crystals," Nat. Phys. **13**, 345–349 (2016).
[20] R. E. F. Silva, I. V. Blinov, A. N. Rubtsov, O. Smirnova, and M. Ivanov, "High-harmonic spectroscopy of ultrafast many-body dynamics in strongly correlated systems," Nat. Photonics **12**, 266–270 (2018).
[21] R. E. F. Silva, A. Jiménez-Galán, B. Amorim, O. Smirnova, and M. Ivanov, "Topological strong-field physics on sub-laser-cycle timescale," Nat. Photonics **13**, 849–854 (2018).
[22] P. B. Corkum, "Plasma perspective on strong field multiphoton ionization," Phys. Rev. Lett. **71**, 1994–1997 (1993).

[23]M. Lewenstein, P. Balcou, M. Y. Ivanov, A. L'Huillier, and P. B. Corkum, "Theory of high-harmonic generation by low-frequency laser fields," Phys. Rev. A **49**, 2117–2132 (1994).
[24]B. Zaks, R. B. Liu, and M. S. Sherwin, "Experimental observation of electron–hole recollisions," Nature **483**, 580–583 (2012).
[25]P. Földi, "Gauge invariance and interpretation of interband and intraband processes in high-order harmonic generation from bulk solids," Phys. Rev. B **96**, 035112 (2017).
[26]X.-Q. Wang, Y. Xu, X.-H. Huang, and X.-B. Bian, "Interference between inter- and intraband currents in high-order harmonic generation in solids," Phys. Rev. A **98**, 023427 (2018).
[27]L. Yue and M. B. Gaarde, "Imperfect recollisions in high-harmonic generation in solids," Phys. Rev. Lett. **124**, 153204 (2020).
[28]N. Yoshikawa, K. Nagai, K. Uchida, Y. Takaguchi, S. Sasaki, Y. Miyata, and K. Tanaka, "Interband resonant high-harmonic generation by valley polarized electron–hole pairs," Nat. Commun. **10**, 3709 (2019).
[29]O. Schubert, M. Hohenleutner, F. Langer, B. Urbanek, C. Lange, U. Huttner, D. Golde, T. Meier, M. Kira, S. W. Koch, and R. Huber, "Sub-cycle control of terahertz high-harmonic generation by dynamical Bloch oscillations," Nat. Photonics **8**, 119–123 (2014).
[30]A. F. Kemper, B. Moritz, J. K. Freericks, and T. P. Devereaux, "Theoretical description of high-order harmonic generation in solids," New J. Phys. **15**, 023003 (2013).
[31]E. N. Osika, A. Chacón, L. Ortmann, N. Suárez, J. A. Pérez-Hernández, B. Szafran, M. F. Ciappina, F. Sols, A. S. Landsman, and M. Lewenstein, "Wannier-Bloch approach to localization in high-harmonics generation in solids," Phys. Rev. X **7**, 021017 (2017).
[32]G. Vampa, C. R. McDonald, G. Orlando, D. D. Klug, P. B. Corkum, and T. Brabec, "Theoretical analysis of high-harmonic generation in solids," Phys. Rev. Lett. **113**, 073901 (2014).
[33]S. M. Teichmann, F. Silva, S. L. Cousin, M. Hemmer, and J. Biegert, "0.5-keV soft X-ray attosecond continua," Nat. Commun. **7**, 11493 (2020).
[34]M. Lara-Astiaso, R. E. Silva, A. Gubaydullin, P. Rivière, C. Meier, and F. Martín, "Enhancing high-order harmonic generation in light molecules by using chirped pulses," Phys. Rev. Lett. **117**, 093003 (2016).
[35]M. Hentschel, R. Kienberger, C. Spielmann, G. A. Reider, N. Milosevic, T. Brabec, P. Corkum, U. Heinzmann, M. Drescher, and F. Krausz, "Attosecond metrology," Nature **414**, 509–513 (2001).
[36]M. Krebs, S. Hädrich, S. Demmler, J. Rothhardt, A. Zaïr, L. Chipperfield, J. Limpert, and A. Tünnermann, "Towards isolated attosecond pulses at megahertz repetition rates," Nat. Photonics **7**, 555–559 (2013).
[37]J. Schötz, B. Förg, W. Schweinberger, I. Liontos, H. A. Masood, A. M. Kamal, C. Jakubeit, N. G. Kling, T. Paasch-Colberg, S. Biswas, M. Högner, I. Pupeza, M. Alharbi, A. M. Azzeer, and M. F. Kling, "Phase-matching for generation of isolated attosecond XUV and soft-x-ray pulses with few-cycle drivers," Phys. Rev. X **10**, 041011 (2020).
[38]G. Vampa, C. R. McDonald, G. Orlando, P. B. Corkum, and T. Brabec, "Semiclassical analysis of high harmonic generation in bulk crystals," Phys. Rev. B **91**, 064302 (2015).
[39]T. T. Luu and H. J. Wörner, "High-order harmonic generation in solids: A unifying approach," Phys. Rev. B **94**, 115164 (2016).
[40]G.-R. Jia, X.-Q. Wang, T.-Y. Du, X.-H. Huang, and X.-B. Bian, "High-order harmonic generation from 2D periodic potentials in circularly and bichromatic circularly polarized laser fields," J. Chem. Phys. **149**, 154304 (2018).
[41]T. Tamaya and T. Kato, "Subband picture of high-harmonic generation in solids," Phys. Rev. B **100**, 081203 (2019).
[42]C. Yu, K. K. Hansen, and L. B. Madsen, "Enhanced high-order harmonic generation in donor-doped band-gap materials," Phys. Rev. A **99**, 013435 (2019).
[43]G. Orlando, T.-S. Ho, and S.-I. Chu, "Simple model of dephasing for high-order harmonic generation in solids," J. Opt. Soc. Am. B **37**, 1540–1549 (2020).
[44]N. F. Aguirre and F. Martín, "Tuning high-harmonic generation by controlled deposition of ultrathin ionic layers on metal surfaces," Phys. Rev. B **94**, 245423 (2016).
[45]H. Nishidome, K. Nagai, K. Uchida, Y. Ichinose, Y. Yomogida, Y. Miyata, K. Tanaka, and K. Yanagi, "Control of high-harmonic generation by tuning the electronic structure and carrier injection," Nano Lett. **20**, 6215–6221 (2020).
[46]T. Huang, X. Zhu, L. Li, X. Liu, P. Lan, and P. Lu, "High-order-harmonic generation of a doped semiconductor," Phys. Rev. A **96**, 043425 (2017).
[47]H. Iravani, K. K. Hansen, and L. B. Madsen, "Effects of vacancies on high-order harmonic generation in a linear chain with band gap," Phys. Rev. Res. **2**, 013204 (2020).
[48]M. S. Mrudul, N. Tancogne-Dejean, A. Rubio, and G. Dixit, "High-harmonic generation from spin-polarised defects in solids," npj Comput. Mater. **6**, 10 (2020).
[49]S. G. Davision and M. Steślicka, *Basic Theory of Surface States* (Oxford University Press, Oxford, 1996).
[50]S. Caratzoulas, B. Jackson, and M. Persson, "Eley–Rideal and hot-atom reaction dynamics of H(g) with H adsorbed on Cu(111)," J. Chem. Phys. **107**, 6420–6431 (1997).
[51]T. Kammler and J. Küppers, "Interaction of H atoms with Cu(111) surfaces: Adsorption, absorption, and abstraction," J. Chem. Phys. **111**, 8115–8123 (1999).
[52]K. Mudiyanselage, Y. Yang, F. M. Hoffmann, O. J. Furlong, J. Hrbek, M. G. White, P. Liu, and D. J. Stacchiola, "Adsorption of hydrogen on the surface and sub-surface of Cu(111)," J. Chem. Phys. **139**, 044712 (2013).
[53]J. Chen, X. Zhou, and B. Jiang, "Eley-Rideal recombination of hydrogen atoms on Cu(111): Quantitative role of electronic excitation in cross sections and product distributions," J. Chem. Phys. **150**, 061101 (2019).
[54]K. Mudiyanselage, S. D. Senanayake, L. Feria, S. Kundu, A. E. Baber, J. Graciani, A. B. Vidal, S. Agnoli, J. Evans, R. Chang, S. Axnanda, Z. Liu, J. F. Sanz, P. Liu, J. A. Rodriguez, and D. J. Stacchiola, "Importance of the metal–oxide interface in catalysis: In situ studies of the water–gas shift reaction by ambient-pressure x-ray photoelectron spectroscopy," Angew. Chem., Int. Ed. **52**, 5101–5105 (2013).
[55]M. Behrens, F. Studt, I. Kasatkin, S. Kühl, M. Hävecker, F. Abild-Pedersen, S. Zander, F. Girgsdies, P. Kurr, B.-L. Kniep, M. Tovar, R. W. Fischer, J. K. Nørskov, and R. Schlögl, "The active site of methanol synthesis over $Cu/ZnO/Al_2O_3$ industrial catalysts," Science **336**, 893–897 (2012).
[56]Y. W. Kim, T.-J. Shao, H. Kim, S. Han, S. Kim, M. Ciappina, X.-B. Bian, and S.-W. Kim, "Spectral interference in high harmonic generation from solids," ACS Photonics **6**, 851–857 (2019).
[57]A. Zaïr, M. Holler, A. Guandalini, F. Schapper, J. Biegert, L. Gallmann, U. Keller, A. S. Wyatt, A. Monmayrant, I. A. Walmsley, E. Cormier, T. Auguste, J. P. Caumes, and P. Salières, "Quantum path interferences in high-order harmonic generation," Phys. Rev. Lett. **100**, 143902 (2008).
[58]T. Auguste, P. Salières, A. S. Wyatt, A. Monmayrant, I. A. Walmsley, E. Cormier, A. Zaïr, M. Holler, A. Guandalini, F. Schapper, J. Biegert, L. Gallmann, and U. Keller, "Theoretical and experimental analysis of quantum path interferences in high-order harmonic generation," Phys. Rev. A **80**, 033817 (2009).
[59]A. K. Kazansky and P. M. Echenique, "One-electron model for the electronic response of metal surfaces to subfemtosecond photoexcitation," Phys. Rev. Lett. **102**, 177401 (2009).
[60]F. Catoire and H. Bachau, "Above-threshold ionization of quasiperiodic structures by low-frequency laser fields," Phys. Rev. Lett. **115**, 163602 (2015).
[61]E. V. Chulkov, V. M. Silkin, and P. M. Echenique, "Image potential states on metal surfaces: Binding energies and wave functions," Surf. Sci. **437**, 330–352 (1999).
[62]E. So, J. A. Gibbard, and T. P. Softley, "Ionization of Rydberg H atoms at band-gap metal surfaces via surface and image states," J. Phys. B: At., Mol. Opt. Phys. **48**, 175205 (2015).
[63]J. J. Carrera and S.-I. Chu, "Extension of high-order harmonic generation cutoff via coherent control of intense few-cycle chirped laser pulses," Phys. Rev. A **75**, 033807 (2007).
[64]A. Taoutioui and H. Agueny, "Femtosecond single cycle pulses enhanced the efficiency of high order harmonic generation," Micromachines **12**, 610 (2021).
[65]J. V. Lill, G. A. Parker, and J. C. Light, "Discrete variable representations and sudden models in quantum scattering theory," Chem. Phys. Lett. **89**, 483–489 (1982).

[66]Q. Liao and U. Thumm, "Attosecond time-resolved photoelectron dispersion and photoemission time delays," Phys. Rev. Lett. **112**, 023602 (2014).
[67]A. L. Cavalieri, N. Müller, T. Uphues, V. S. Yakovlev, A. Baltuška, B. Horvath, B. Schmidt, L. Blümel, R. Holzwarth, S. Hendel, M. Drescher, U. Kleineberg, P. M. Echenique, R. Kienberger, F. Krausz, and U. Heinzmann, "Attosecond spectroscopy in condensed matter," Nature **449**, 1029–1032 (2007).
[68]M. Lewenstein, K. C. Kulander, K. J. Schafer, and P. H. Bucksbaum, "Rings in above-threshold ionization: A quasiclassical analysis," Phys. Rev. A **51**, 1495–1507 (1995).
[69]M. Bellini, C. Lyngå, A. Tozzi, M. B. Gaarde, T. W. Hänsch, A. L'Huillier, and C.-G. Wahlström, "Temporal coherence of ultrashort high-order harmonic pulses," Phys. Rev. Lett. **81**, 297–300 (1998).
[70]D. Gauthier *et al.*, "Chirped pulse amplification in an extreme-ultraviolet free-electron laser," Nat. Commun. **7**, 13688 (2016).
[71]D. Strickland and G. Mourou, "Compression of amplified chirped optical pulses," Opt. Commun. **56**, 219–221 (1985).
[72]F. X. Kärtner, U. Morgner, R. Ell, T. Schibli, J. G. Fujimoto, E. P. Ippen, V. Scheuer, G. Angelow, and T. Tschudi, "Ultrabroadband double-chirped mirror pairs for generation of octave spectra," J. Opt. Soc. Am. B **18**, 882–885 (2001).
[73]K.-H. Hong, J. H. Sung, Y. S. Lee, and C. H. Nam, "Temporal characterization of chirped femtosecond laser pulses," Opt. Commun. **213**, 193–200 (2002).
[74]T. S. Clement, D. J. Kane, and A. J. Taylor, "Single-shot measurement of the amplitude and phase of ultrashort laser pulses in the violet," Opt. Lett. **20**, 70–72 (1995).